Nested formation mechanisms of Fano line shape in far-field response of coupled waveguide multilayer structure revealed by analyses of local electric fields

Hayashi, Shinji
Motokura, Kengo
Fujii, Minoru
Nesterenko, Dmitry V.
Sekkat, Zouheir

(Citation)
Journal of Applied Physics,132(16):163104

(Issue Date)
2022-10-28

(Resource Type)
journal article

(Version)
Version of Record

Journal of Applied Physics

Nested formation mechanisms of Fano line shape in far-field response of coupled waveguide multilayer structure revealed by analyses of local electric fields

Cite as: J. Appl. Phys. **132**, 163104 (2022); https://doi.org/10.1063/5.0097031
Submitted: 25 April 2022 • Accepted: 28 September 2022 • Published Online: 27 October 2022

Shinji Hayashi, Kengo Motokura, Minoru Fujii, et al.

Journal of Applied Physics ARTICLE scitation.org/journal/jap

Nested formation mechanisms of Fano line shape in far-field response of coupled waveguide multilayer structure revealed by analyses of local electric fields

Cite as: J. Appl. Phys. **132**, 163104 (2022); doi: 10.1063/5.0097031
Submitted: 25 April 2022 · Accepted: 28 September 2022 ·
Published Online: 27 October 2022

Shinji Hayashi,[1,2,a)] Kengo Motokura,[1] Minoru Fujii,[1] Dmitry V. Nesterenko,[3,4] and Zouheir Sekkat[2,5]

AFFILIATIONS

[1]Department of Electrical and Electronic Engineering, Graduate School of Engineering, Kobe University, Kobe 657-8501, Japan
[2]Optics and Photonics Center, Moroccan Foundation for Science, Innovation and Research (MAScIR), University Mohammed VI Polytechnic, Rabat 10100, Morocco
[3]Image Processing Systems Institute RAS—Branch of the FSRC "Crystallography and Photonics" RAS, Samara 443001, Russia
[4]Faculty of Information Technology, Samara National Research University, Samara 443086, Russia
[5]Faculty of Sciences, Mohamed V University in Rabat, Rabat 10010, Morocco

[a)]**Author to whom correspondence should be addressed:** s.hayashi@dragon.kobe-u.ac.jp

ABSTRACT

Based on electromagnetic calculations, the formation mechanism of the Fano line shape in the attenuated total reflection (far-field) spectrum of a coupled waveguide multilayer structure is studied in detail by tracing back to the behaviors of local electric fields. The Fano line shape of absorptance A directly related to the reflectance by $R = 1 - A$ is shown to be generated by a superposition of a Fano line shape exhibited by local absorption in one of the waveguide layers and a Lorentzian line shape exhibited by local absorption in another waveguide layer. It is also shown that the Fano line shape of the first waveguide layer is generated by a superposition of different Fano line shapes exhibited by local electric fields at different positions inside the waveguide layer. These results unveil the nested mechanisms of the Fano line shape formation hidden in the behaviors of local electric fields. The Fano resonance inside the first waveguide layer is thought to be an example of the multiple Fano resonance arising from the interaction between multiple continua with a discrete state.

I. INTRODUCTION

Over the past decade, Fano resonances generated in optical responses of metallic and dielectric nanostructures have been widely investigated both experimentally and theoretically, since the steep part of asymmetric line shapes associated with the resonances is very much promising to develop high-performance devices, such as optical sensors and switches based on tailored nanostructures.[1–3] As early as in 1935, the asymmetric line shapes observed in atomic spectra were analyzed by Ugo Fano and explained in terms of the interference between a discrete quantum state and a continuum.[4,5] He derived the following simple line shape function, called the Fano formula, that describes the asymmetric line shape as a function of photon energy E with the aid of an asymmetry parameter q,

$$\sigma_F = \sigma_0 \frac{(X+q)^2}{X^2+1}, \tag{1}$$

where X is given by $X = \frac{E-E_F}{\Gamma}$ with the resonance energy E_F and the half width of the resonance Γ, and σ_0 represents the background intensity. In Fano-resonant nanostructures, the generation of the Fano line shape in far-field optical responses is commonly interpreted as due to the interference of pathways governed by a broad (bright) electromagnetic (EM) mode and a sharp (dark) EM

mode. In recent years, various aspects of the Fano line shape including the generalization of the Fano formula to cover cases with losses,[6–8] transition from the Lorentzian to Fano line shape,[9–11] and the necessity of introducing complex q[12–14] have been the subjects of intensive research.

It is common to investigate Fano line shapes appearing in far-field responses of nanostructures such as scattering, transmission, and reflection spectra. Normally, behaviors of local fields or near fields inside or in the vicinity of building blocks of nanostructures are not pursued deeply. In general, the relationship between the far-field spectra and the behavior of local fields or near fields is complex. However, as pointed out by Gallinet and Martin,[8] spectra of local fields or near fields associated with excitation of the bright EM mode can exhibit Fano line shapes, and they play an essential role in generating Fano line shapes in far-field responses. Experimental observation of local fields or near fields is difficult except for rare cases to which sophisticated experimental techniques, such as cathodoluminescence and scanning near-field microscopy, are applicable. Due partly to the experimental difficulty, behaviors of local fields or near fields in Fano-resonant nanostructures in relation with the far-field responses have not been studied in detail so far. However, detailed studies of local fields or near fields in Fano-resonant nanostructures are indispensable not only to fully understand the formation mechanism of Fano line shapes in far-field spectra but also to extend the applicability of the Fano resonance to devices operating with local fields or near fields, such as platforms of enhanced spectroscopies and optical sensors.

Very recently, we have demonstrated that Fano-resonant behaviors of local electric fields inside one of two waveguide layers in a coupled waveguide structure can be monitored by measuring the fluorescence excitation spectra of dye molecules doped into the waveguide layer.[15] In our experiments, the waveguide layer supporting the broad waveguide mode was doped with fluorescent dye molecules and the intensity of the fluorescence from the molecules was measured by exciting the molecules in an attenuated total reflection (ATR) geometry. The measured fluorescence excitation spectrum exhibited the Fano line shape, which is very similar to that appearing in the ATR spectrum turned upside down. Based on EM calculations, we showed that the fluorescence excitation spectrum agrees very well with the behavior of local electric fields integrated over the waveguide layer. Although the similarity between the ATR spectrum (far-field spectrum) and the fluorescence excitation spectrum (integral behavior of local electric fields) suggests an important contribution of the local electric fields to the far-field response, in the previous work, detailed behaviors of the local electric fields such as their position dependence and changes in the line shape of their intensity spectra have not been performed, leaving the roles of the local electric fields in forming the far-field line shape unknown.

To clarify the relationship between the far-field spectrum and the behavior of local electric fields and reveal the formation mechanism of Fano line shape at the level of local electric fields, we performed comprehensive analyses of the far-field ATR spectrum and local electric fields, assuming a coupled waveguide multilayer structure very similar to that used in our previous experiments. In this paper, we report doubly nested formation mechanisms of Fano line shape, unveiled with the aid of EM calculations of electric field distributions inside the structure and spectral fitting with Fano line shape functions. We show that in the Fano line shape of the far-field ATR spectrum, two components, a Fano line shape and a Lorentzian line shape, are hidden. Furthermore, we show that the Fano line shape originating from local absorption in the first waveguide layer is generated by a superposition of different Fano line shapes exhibited by local electric fields at different positions. These conclusions drawn from spectral fitting are discussed in light of mathematical considerations.

II. RESULTS AND DISCUSSION

A. Fano and Lorentzian line shapes hidden in far-field ATR response

In this work, we consider the Fano-resonant all-dielectric multilayer structure schematically shown in Fig. 1(a); the structure is similar to that used in our previous experimental studies of ATR and fluorescence spectra.[15,16] The structure consists of two waveguide layers, denoted as WG1 and WG2 layers, separated by a spacer layer, denoted as the S2 layer, integrated in an ATR

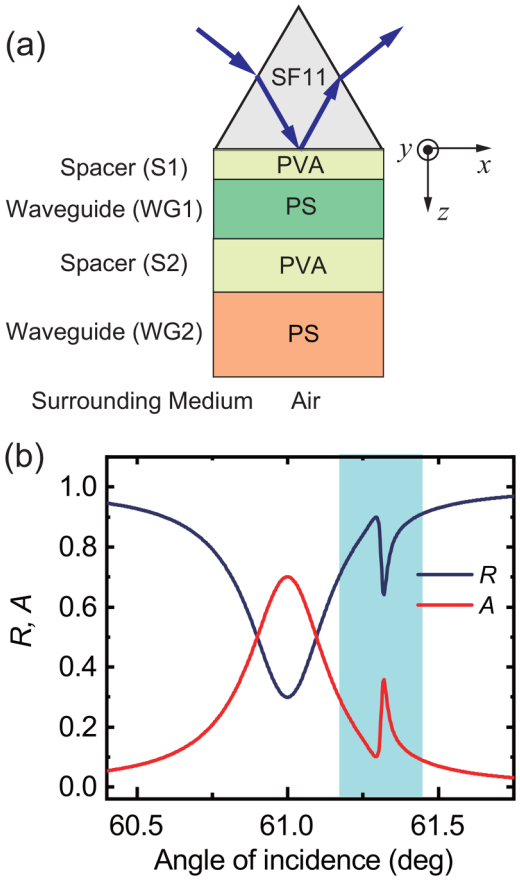

FIG. 1. (a) ATR configuration of Fano-resonant multilayer structure assumed. (b) Calculated spectra of reflectance R and absorptance A ($=1-R$).

geometry. In our previous experimental studies,[15,16] the waveguide layers and spacer layers were made of polystyrene (PS) and polyvinyl alcohol (PVA), respectively, prepared by a spin coating method. A prism made of SF11 glass was used as a high-index dielectric layer that allows coupling of the incident light to nonradiative EM modes of the multilayer system mediated by an evanescent wave generated in the first spacer layer, denoted as the S1 layer. The Fano resonances were observed in the angle-scan ATR spectra. The Fano resonances were also observed in fluorescence spectra by doping the WG1 layer with fluorescent dye molecules. In the present work, to make the analysis realistic, we assume the same sets of materials for the prism, waveguide and spacer layers, and surrounding medium. However, for simplicity, we assume round numbers for the wavelength of the incident light and the thicknesses of the layers. The wavelength of the incident light assumed is $\lambda = 450$ nm and the refractive indices of the PS and PVA layers were taken from Ref. 17. The structural parameters used in the present EM calculations are listed in Table I. Very small values were assumed for the extinction coefficients of the S1 and S2 layers. Furthermore, to generate a broad waveguide mode, a relatively large value of the extinction coefficient was assumed for the WG1 layer, while a relatively small value was assumed for the WG2 layer to generate a sharp waveguide mode. The surrounding medium was assumed to be air. As discussed in detail in our previous papers,[15,16] the Fano resonances in the analyzed structure originate from the coupling between a broad planar waveguide mode supported by the WG1 layer (PWG1 mode) and a sharp planar waveguide mode supported by the WG2 layer (PWG2 mode). As shown in Fig. 1(a), the z axis is assumed to be normal to the interfaces and the prism/S1 interface is set at $z = 0$. The PWG1 and PWG2 modes propagating along the x axis are assumed to be excited by a plane wave incident in the $x - z$ plane.

Normally, the Fano resonances in nanostructures appear in far-field responses. For the present multilayer structure, the relevant far-field response is the reflectance spectrum measured under the total reflection condition, i.e., the ATR spectrum. Using a 2×2 transfer matrix method[18] together with the parameters listed in Table I, we calculated the angle-scan ATR spectrum. An s-polarized plane wave was assumed to be incident on the multilayer stack through the SF11 prism and the reflectance R was calculated as a function of the angle of incidence θ_{in}. Figure 1(b) shows the ATR spectrum obtained. In the figure, we see a broad dip around 61.0°, which is attributed to the excitation of the PWG1 mode. Furthermore, we see clearly an asymmetric line shape located around 61.3°, a Fano line shape. In general, for a planar multilayer system, energy conservation requires $R + A + T = 1$, where A and T are the absorptance and transmittance, respectively. Since the ATR spectrum is obtained under the total reflection condition, $T = 0$ holds, and consequently, the absorptance is given by $A = 1 - R$. The spectrum of A converted from that of R is also shown in Fig. 1(b); the spectrum shows clearly an asymmetric Fano line shape turned upside down. The origin of the Fano resonance in the far-field response R can, thus, be traced back to that in A, which is determined by the total absorption in the multilayer structure.

TABLE I. Structural parameters assumed.

Layer	Thickness (nm)	Refractive index
SF11	Infinite	1.8192
S1	190	$1.4975 + i1.0 \times 10^{-5}$
WG1	600	$1.6136 + i2.0 \times 10^{-3}$
S2	300	$1.4975 + i1.0 \times 10^{-5}$
WG2	760	$1.6136 + i1.0 \times 10^{-4}$
Air	Infinite	1.0

To investigate in detail the roles played by local electric fields to generate the line shape in the far-field ATR response, we also calculated distributions of electric fields induced inside the layers under the ATR excitation using the 2×2 transfer matrix method. We define the field enhancement factor (FEF) at the position z inside the structure by $FEF(z, \theta_{in}) = |E_s(z, \theta_{in})|^2 / |E_0|^2$, where $E_s(z, \theta_{in})$ is the amplitude of the local electric field and E_0 is that of the electric field of the incident wave. $FEF(z, \theta_{in})$ was calculated for various z by varying θ_{in}. As in our previous study,[15] in discussing the resonant behaviors of $FEF(z, \theta_{in})$, it is appropriate to use the in-plane wavevector instead of θ_{in}. The in-plane wavevector is given by $k_x = k_0 n_{SF11} \sin\theta_{in}$ with $k_0 = 2\pi/\lambda$, where λ is the wavelength of the incident light and n_{SF11} is the refractive index of the SF11 glass. For convenience, in this paper, we use a normalized in-plane wavevector $\alpha = k_x/k_0$ and plot FEF as a function of α and z [$FEF(z, \alpha)$].

The map of FEF obtained is shown in Fig. 2. As can be seen in the figure, FEF inside the WG1 layer exhibits a broad distribution spread over a wide range of α corresponding to the excitation

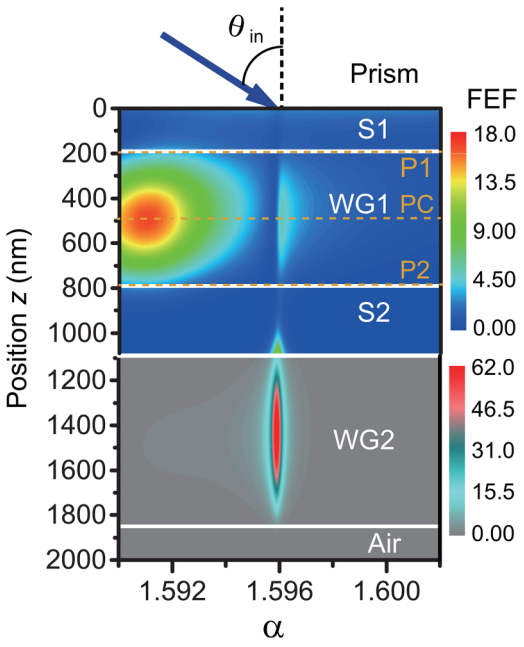

FIG. 2. Map of FEF calculated by the 2×2 transfer matrix method.

of a broad TE_0 waveguide mode. A salient feature in the distribution is splitting into two parts separated by a narrow low FEF region around $\alpha = 1.5956$. In contrast to the distribution inside the WG1 layer, the WG2 layer exhibits a distribution highly localized around $\alpha = 1.5959$ with a maximum FEF as large as 62; this distribution is attributed to the excitation of a sharp TE_0 waveguide mode inside the WG2 layer. The suppression of FEF inside the WG1 layer around $\alpha = 1.5956$ is due to the energy transfer from the PWG1 mode to the PWG2 mode caused by the coupling of the modes mediated by evanescent waves inside the S2 layer.

According to the EM theory,[19] the energy of light absorbed per unit time and unit volume in the vicinity of a point $\mathbf{r} = (x, y, z)$ inside an absorptive medium is proportional to $\varepsilon_2|\mathbf{E}_{loc}(\mathbf{r})|^2$, where ε_2 is the imaginary part of the dielectric constant of the medium and $\mathbf{E}_{loc}(\mathbf{r})$ is the local electric field at the point $\mathbf{r}$. Based on this relationship, we can estimate the energy absorbed in a layer in our multilayer structure by $A_{layer}(\alpha) = C\int_d \varepsilon_2 FEF(z, \alpha)dz$, where the integral is taken over the layer thickness d and C is a proportionality constant. In this expression, a factor $(\cos\theta_{in})^{-1}$ describing the variation of the incident energy per unit area was omitted, since the variation is negligibly small in a narrow angle region around the Fano resonance. Using the numerical data of $FEF(z, \alpha)$, we calculated separately $A_{layer}(\alpha)$ for all layers and summed them up to obtain the total energy absorbed $A_T(\alpha)$. In calculating numerically the integrals, the data of $FEF(z, \alpha)$ for the positions z separated by 1 nm inside each layer were summed up. After adjusting the proportionality constant C so that the maximum value of $A_T(\alpha)$ coincides with that of the spectrum of A in Fig. 1(b), the spectrum of $A_T(\alpha)$ is shown in Fig. 3 together with those of $A_{WG1}(\alpha)$ and $A_{WG2}(\alpha)$ for the WG1 and WG2 layers, respectively. In this figure, $A_{S1}(\alpha)$ and $A_{S2}(\alpha)$ for the S1 and S2 layers are not shown, because their maximum values are three orders of magnitude smaller than that of $A_T(\alpha)$ due to the small extinction coefficients and small FEF in these layers, and their contributions to $A_T(\alpha)$ are negligibly small. It should be noted that the spectrum of $A_T(\alpha)$ in Fig. 3 obtained from the electric field distributions reproduces very well that of A in Fig. 1(b) obtained from the reflectance spectrum.

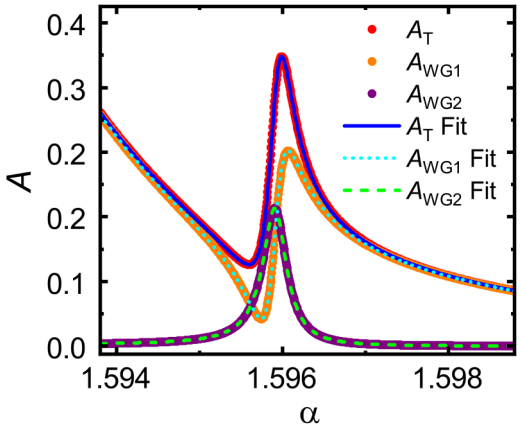

FIG. 3. Spectra of absorption calculated from distributions of local electric fields, corresponding to WG1 layer $A_{WG1}(\alpha)$ and WG2 layer $A_{WG2}(\alpha)$, and total absorption $A_T(\alpha)$ given by a summation of absorption in all layers. Results of fitting to line shape function (fit curves) are also shown.

To extract the resonance characteristics of the spectra shown in Fig. 3, we fit them with line shape functions. For the asymmetric Fano line shape, we adopt the following formula, which is more general than the original Fano formula [Eq. (1)],

$$\sigma_F = \frac{(X+q)^2 + b}{X^2 + 1}. \tag{2}$$

This generalized Fano formula was derived by Gallinet and Martin from an *ab initio* theory for EM scattering in general dispersive and lossy media.[6] They showed that this formula can also be obtained from a model of coupled harmonic oscillators with losses as an approximate expression of the oscillator amplitude around the resonance.[6,20] In addition to the asymmetry parameter q, Eq. (2) contains a modulation damping parameter b, which describes the screening of the resonance caused by intrinsic losses. With a variable α, which represents either the photon energy E or radial frequency ω of light wave, or alternatively the normalized in-plane wavevector of incident wave used in this paper, X is defined by $X = (\alpha^2 - \alpha_F^2)/\Gamma_F$ with α_F and Γ_F denoting the resonance position and width, respectively.

Like the spectrum of A shown in Fig. 1(b), asymmetric line shapes observed in nanostructures are often superposed on a broad background. In this case, it is appropriate to express the total line shape as

$$\sigma(\alpha) = \sigma_B(\alpha)\sigma_F(\alpha), \tag{3}$$

where $\sigma_B(\alpha)$ is the line shape function of the background. In fitting the absorption spectra shown in Fig. 3, we need a functional form of $\sigma_B(\alpha)$. As explained in detail later, to achieve high-quality fitting, we attempted to fit the spectra only in a narrow region around the Fano resonance, in which the background intensities vary slowly. Among a variety of choices for the slowly varying background function, following the derivation of the generalized Fano function from the coupled oscillator model described in Refs. 6 and 20, we choose the following form of the background function that normally describes the response of an harmonic oscillator driven by an external force:

$$\sigma_B(\alpha) = \frac{f^2}{|\,\alpha_1^2 - \alpha^2 + i\gamma\alpha\,|^2}, \tag{4}$$

where f is the amplitude of the external force acting on an oscillator generating the broad background, and α_1 and γ are the resonance position and damping constant of the oscillator, respectively. We note that although Eq. (4) describes a Lorentzian line shape when it is applied to the whole spectral range, the parameters obtained from our fitting in a narrow range are expected to well reproduce only the slowly varying part of the background intensities, but fail to reproduce the whole Lorentzian line shape corresponding to the excitation of the PWG1 mode. Using the line shape function given by Eq. (3) together with Eqs. (2) and (4), we performed the fitting for the asymmetric spectra of $A_T(\alpha)$ and

TABLE II. Fitting parameters obtained for absorption spectra.

Spectra	f	α_1	γ	α_F or α_L	Γ_F or Γ_L	q	b
A_T	$6.303\,21 \times 10^{-3}$	1.591 26	$4.685\,66 \times 10^{-3}$	1.595 91	$5.572\,77 \times 10^{-4}$	0.766 114	1.591 65
A_{WG1}	$6.292\,30 \times 10^{-3}$	1.591 26	$4.684\,64 \times 10^{-3}$	1.595 91	$5.565\,94 \times 10^{-4}$	0.776 042	0.392 201
A_{WG2}	$5.498\,64 \times 10^{-3}$	1.592 22	$3.913\,11 \times 10^{-3}$	1.595 91	$5.566\,83 \times 10^{-4}$	…	…

$A_{WG1}(\alpha)$ in Fig. 3. In fitting the symmetric spectrum of $A_{WG2}(\alpha)$, we assumed the same functional form of $\sigma_B(\alpha)$, but the generalized Fano function $\sigma_F(\alpha)$ was replaced by a Lorentzian function simply given by $\sigma_L(\alpha) = \frac{1}{X^2+1}$. This form of the Lorentzian function was chosen to retain its similarity to the generalized Fano function given by Eq. (2) and to facilitate the mathematical considerations given later. The resonance position and width of the Lorentzian line shape are denoted as α_L and Γ_L, respectively.

To obtain fitting results with high accuracy, we fitted the absorption spectra shown in Fig. 3 by limiting the fitting range to a narrow interval of $1.5930 \leq \alpha \leq 1.5990$ around the Fano resonance. The fit parameters obtained from a nonlinear least squares method are given in Table II. The fit curves calculated by the line shape functions using the fit parameters are presented in Fig. 3. We see that all the fit curves reproduce very well the absorption spectra; the fitting errors are too small to be seen in the figure. Fitting errors were estimated by introducing a maximum relative error defined by $\varepsilon_{max} = max|D(\alpha) - \sigma_{fit}(\alpha)|/maxD(\alpha)$, where $D(\alpha)$ stands for $A_T(\alpha)$, $A_{WG1}(\alpha)$, and $A_{WG2}(\alpha)$, and $\sigma_{fit}(\alpha)$ represents the corresponding fit curves. Values of ε_{max} obtained for $A_T(\alpha)$, $A_{WG1}(\alpha)$ and $A_{WG2}(\alpha)$ are as small as 0.027%, 0.043%, and 0.028%, respectively, indicating high quality of the present fitting. It is now clear that in the Fano line shape of $A_T(\alpha)$ directly related to the far-field ATR spectrum, the Fano line shape of $A_{WG1}(\alpha)$ and the Lorentzian line shape of $A_{WG2}(\alpha)$ are hidden. This finding is summarized in the upper half of Fig. 4.

B. Fano line shapes hidden in average local-field response of WG1 layer

As demonstrated in Sec. II A, the Fano line shape of $A_{WG1}(\alpha)$ plays an essential role to generate the Fano line shape of $A_T(\alpha)$, which in turn generates the Fano line shape in the far-field ATR spectrum. Since $A_{WG1}(\alpha)$ reflects the integral behavior of local electric fields inside the WG1 layer, to understand in depth the origin of the far-field Fano line shape, it is necessary to clarify behaviors of local electric fields at different positions inside the WG1 layer. In this subsection, we focus on them and reveal the Fano line shapes hidden in their integral or average behavior represented by $A_{WG1}(\alpha)$.

To see clearly the behavior of FEF inside the WG1 layer, spectra of $FEF(z, \alpha)$ corresponding to three different sampling points are shown in Fig. 5(a); the sampling points are specified by $z = 191$, 490, and 789 nm, which are located at 1 nm away from the S1/WG1 interface, the center of the layer and 1 nm away from the WG1/S2 interface. Hereafter, these sampling points are denoted as P1, PC, and P2, respectively. In the figure, an average spectrum obtained by averaging the spectra of 600 sampling points separated by 1 nm inside the WG1 layer is also shown. It should be noted that when an appropriate constant is multiplied, this average spectrum coincides with that of $A_{WG1}(\alpha)$ in Fig. 3. Figure 5(a) shows that all these spectra exhibit asymmetric line shapes. A remarkable feature seen in this figure is the change in the line shape depending on the sampling point. The spectra are shown separately in expanded scales in Figs. 5(b) and 5(c). They demonstrate more clearly the spectral changes. In contrast to this, the line shape of $FEF(z, \alpha)$ inside the WG2 layer does not change depending on the sampling point. According to our detailed analyses, the resonance position and the width of their Lorentzian line shape do not depend on the sampling position and only the peak height changes depending on the sampling point.

For all the spectra shown in Fig. 5, we performed fitting to the Fano line shape function given by Eqs. (2)–(4). The fitting parameters obtained are listed in Table III. The fit curves calculated with the fitting parameters are also shown in Figs. 5(b)–5(e). We see that the fit curves reproduce very well the FEF spectra, and fitting errors are too small to be seen in the figures. The maximum relative errors estimated in the same manner as for the absorption spectra are 0.61%, 0.27%, and 0.37% for the $FEF(z, \alpha)$ spectra at P1, PC, and P2 sampling positions, respectively, and 0.043% for the average spectrum. These values indicate again the high quality of the fitting.

Spectra of the background and Fano functions for the different sampling points $[\sigma_B^j(\alpha)$ and $\sigma_F^j(\alpha)]$ calculated using the fitting parameters (Table III) are plotted in Figs. 6(a) and 6(b), respectively. As we see in Fig. 6(a), $\sigma_B^j(\alpha)$ decreases monotonously with increasing α. In the inset of Fig. 6(a), the background functions normalized to their values at the Fano resonance $\alpha_F = 1.595\,91$, written as $\sigma_B^{jN}(\alpha) = \sigma_B^j(\alpha)/\sigma_B^j(\alpha_F)$, are plotted in the vicinity of the resonance. We see that the slope of the normalized background function $\sigma_B^{jN}(\alpha)$ is almost identical independent of the sampling point, although the value of $\sigma_B^j(\alpha_F)$ varies strongly depending on the sampling point. In Fig. 6(b), we see clearly the strong dependence of $\sigma_F^j(\alpha)$ on the sampling point; the average line shape is very close to that of the center. For $FEF(\alpha)$ spectra of 600 different sampling points $z = z_j$ separated by 1 nm inside the WG1 layer, the same fitting procedure was carried out and the fitting parameters were obtained. The normalization factor $\sigma_B^j(\alpha_F)$ for the background function and the parameters q_j and b_j for the Fano function, extracted from the fitting results, are plotted as a function of z_j in Figs. 6(c), 6(d), and 6(e), respectively. Figures 6(d) and 6(e) demonstrate that q_j varies strongly depending on the sampling point, while b_j varies only slightly. Therefore, the changes seen in the spectra of $\sigma_F^j(\alpha)$ [Fig. 6(b)] are mainly caused by the variation in q_j.

The results presented above clearly demonstrate that the spectra of local electric fields at different positions inside the WG1

layer, represented by $FEF(z_j, \alpha)$, exhibit different Fano line shapes with different values of q_j, and the spectrum averaged over the layer also exhibits a Fano line shape. This implies that a superposition of the different Fano line shapes becomes also a Fano line shape. In other words, the different Fano line shapes are hidden in the average Fano line shape. Since the absorption spectrum inside the WG1 layer $A_{WG1}(\alpha)$ is proportional to the average spectrum, we can finally conclude that the different Fano line shapes inside the WG1 layer make essential contributions to generate the Fano line shape in the far-field ATR response. As summarized in Fig. 4, the present analyses reveal the doubly nested mechanisms of line shape formation in the Fano resonance of far-field response of the multilayer structure.

C. Mathematical considerations

1. Superposition of Fano and Lorentzian line shapes

First, let us consider a simple weighted sum of a Fano function and a Lorentzian function, without taking into account the background functions, written as

$$\hat{\sigma}(\alpha) = w\sigma_F(\alpha) + v\sigma_L(\alpha), \tag{5}$$

where w and v are the weights for the respective line shape functions. Inserting the Fano function given by Eq. (2) and the Lorentzian function given by $\sigma_L(\alpha) = \frac{1}{X^2+1}$ into the above equation and assuming that the resonance positions and widths of both line shapes are identical ($\alpha_F = \alpha_L$ and $\Gamma_F = \Gamma_L$), it is easy to derive the following equation:

$$\hat{\sigma}(\alpha) = w\frac{(X+q)^2 + (b+\frac{v}{w})}{X^2+1}. \tag{6}$$

This result implies that even after the addition of the Lorentzian line shape, the Fano line shape remains a Fano line shape; the addition of the Lorentzian line shape results in the increase in the parameter b by $\Delta b = \frac{v}{w}$ without changing the parameter q. We note here that the above result corroborates with that of Avrutsky *et al.*,[9] when b is set to zero.

We now take into account the background functions, $\sigma_B^F(\alpha)$ for the Fano line shape and $\sigma_B^L(\alpha)$ for the Lorentzian line shape,

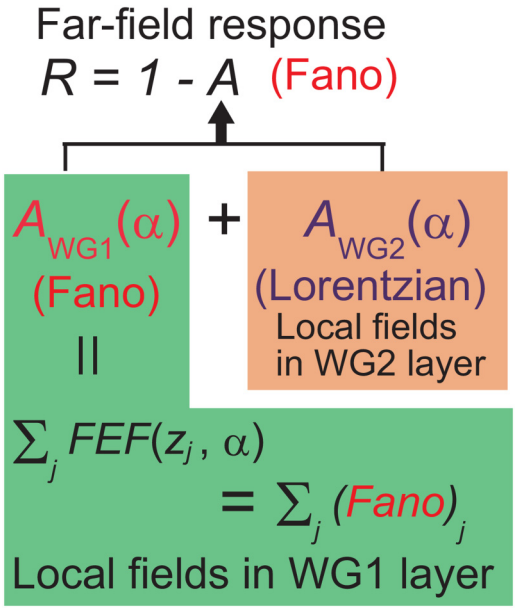

FIG. 4. Nested formation mechanisms of Fano line shapes unveiled from detailed analyses of local electric fields inside WG1 and WG2 waveguide layers.

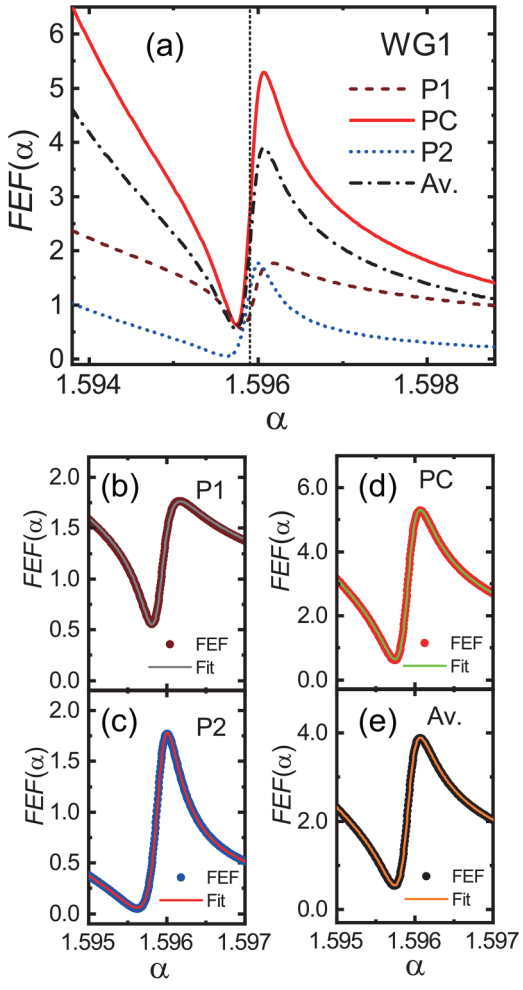

FIG. 5. (a) Spectra of $FEF(z, \alpha)$ in the vicinity of $\alpha = 1.5959$ for sampling points P1, P2, and PC inside the WG1 layer. The average spectrum is also shown. They are shown separately in expanded scales for sampling points P1 (b), P2 (c), and PC (d) and for average spectrum (e). In (b)–(e), dots represent spectra of $FEF(\alpha)$ and solid lines are fit curves obtained from fitting to Fano line shape function.

TABLE III. Fitting parameters obtained.

Position	f	α_1	γ	α_F	Γ_F	q	b
P1	$3.925\,15 \times 10^{-2}$	1.586 02	$3.769\,44 \times 10^{-12}$	1.595 91	$5.634\,71 \times 10^{-4}$	0.361 343	0.417 697
PC	$2.753\,62 \times 10^{-2}$	1.591 58	$4.472\,87 \times 10^{-3}$	1.595 91	$5.538\,23 \times 10^{-4}$	0.802 660	0.345 721
P2	$9.973\,33 \times 10^{-3}$	1.592 01	$3.984\,28 \times 10^{-3}$	1.595 92	$5.557\,13 \times 10^{-4}$	1.540 249	0.371 845
Average	$2.529\,07 \times 10^{-2}$	1.591 26	$4.684\,64 \times 10^{-3}$	1.595 91	$5.565\,94 \times 10^{-4}$	0.776 042	0.392 201

respectively, and consider a total line shape given by

$$\sigma_T(\alpha) = \sigma_B^F(\alpha)\sigma_F(x) + \sigma_B^L(\alpha)\sigma_L(\alpha). \tag{7}$$

We introduce normalized background functions $\sigma_B^{NF}(\alpha)$ and $\sigma_B^{NL}(\alpha)$ normalizing the original background functions to their values at the resonance positions α_F and α_L given by $w_F = \sigma_B^F(\alpha_F)$ and $v_L = \sigma_B^L(\alpha_L)$. In general, $\sigma_B^{NF}(\alpha)$ and $\sigma_B^{NL}(\alpha)$ can have different functional forms, but we assume here that they can be expressed by a common function $g(\alpha)$ as $\sigma_B^{NF}(\alpha) = \sigma_B^{NL}(\alpha) = 1/g(\alpha)$. Then, we can write the background functions as $\sigma_B^F(\alpha) = \sigma_B^F(\alpha_F)\sigma_B^{NF}(\alpha) = w_F/g(\alpha)$ and $\sigma_B^L(\alpha) = \sigma_B^L(\alpha_L)\sigma_B^{NL}(\alpha) = v_L/g(\alpha)$. Inserting these expressions of the background functions into Eq. (7), we can obtain finally the following equation similar to Eq. (6):

$$\sigma_T(\alpha) = \frac{w_F}{g(\alpha)} \frac{(X+q)^2 + (b + \frac{v_L}{w_F})}{X^2+1}. \tag{8}$$

This equation suggests that the increase Δb in the parameter b is now related to the values of the background functions at the resonance positions, w_F and v_L, by $\Delta b = \frac{v_L}{w_F}$.

The above considerations suggest that a superposition of a Fano line shape and a Lorentzian line shape becomes a Fano line shape, provided that the necessary conditions mentioned above are satisfied. This conclusion is mathematically rigorous. However, returning back to the fitting results of the absorption spectra described in Sec. II A, we find that in practice, the spectrum of $A_T(\alpha)$ given by the superposition of $A_{WG1}(\alpha)$ (Fano line shape)

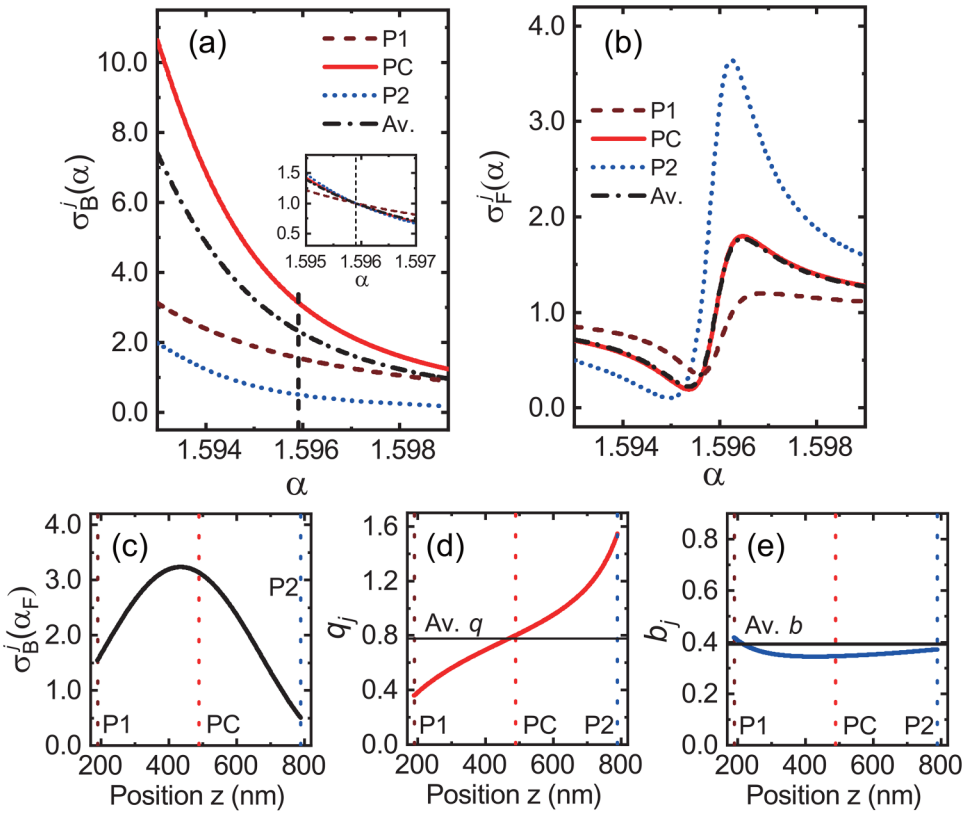

FIG. 6. Background functions $\sigma_B^j(\alpha)$ (a) and generalized Fano functions $\sigma_F^j(\alpha)$ (b), determined for spectra of P1, PC, and P2 sampling points as well as for average spectrum. Position dependencies of normalization factor of background function $\sigma_B^j(\alpha_F)$ (c), asymmetry parameter q_j (d), and modulation damping parameter b_j (e).

and $A_{WG2}(\alpha)$ (Lorentzian line shape) can be fitted very well by the Fano line shape function with very small errors, even though they do not satisfy rigorously the necessary conditions. A close examination of the fit parameters listed in Table II reveals that α_F is identical to α_L, while Γ_F deviates slightly from Γ_L, indicating that the conditions for the Fano and Lorentzian functions are satisfied only approximately. From detailed analyses of the background functions for $A_{WG1}(\alpha)$ and $A_{WG2}(\alpha)$ calculated by their fitting parameters, we found that around the resonance positions, the background intensities decrease almost linearly with α; when the functions are normalized to their values at the resonance positions, they are almost identical. This implies that the assumption of the common functional form for the normalized background functions is also approximately satisfied. An estimate of Δb obtained from w_F and v_L values of the normalized background functions is 1.183 53, which is close to 1.199 45 obtained from the b values listed in Table II. The discrepancy between these estimates stems from the fact that the analyzed spectra do not satisfy rigorously the mathematically required conditions. Nevertheless, the present analyses of the absorption spectra demonstrate that the addition of the Lorentzian line shape to the Fano line shape results in the Fano line shape with practically the same q factor and the increased b factor, in good agreement (at least qualitatively) with the rigorous mathematical prediction.

2. Superposition of different Fano line shapes

We now proceed to the discussion on the Fano line shape generated by a superposition of different Fano line shapes. Let us consider a set of generalized Fano function $\sigma_F^j(\alpha)$ $(j = 1, \ldots, N)$ written in the form of Eq. (2) with different parameters q_j and b_j. We assume that the resonance position α_F and the width of the resonance Γ_F are constants common for all $\sigma_F^j(\alpha)$. The background functions are taken into account later. A superposition of $\sigma_F^j(\alpha)$ with weights w_j is written as

$$\hat{\sigma}_F(\alpha) = \sum_{j=1}^{N} w_j \sigma_F^j(\alpha) = \sum_{j=1}^{N} w_j \frac{(X+q_j)^2 + b_j}{X^2+1}. \tag{9}$$

It is straightforward to show that $\hat{\sigma}_F(\alpha)$ takes the form of the generalized Fano formula with new parameters Q and B. In fact, in terms of averages $\bar{q} = \frac{1}{W}\sum_{j=1}^{N} w_j q_j$, $\bar{q^2} = \frac{1}{W}\sum_{j=1}^{N} w_j q_j^2$, and $\bar{b} = \frac{1}{W}\sum_{j=1}^{N} w_j b_j$, where W is the total weight $W = \sum_{j=1}^{N} w_j$, we can express as

$$\hat{\sigma}_F(\alpha) = W \frac{(X+Q)^2 + B}{X^2+1}, \tag{10}$$

with new parameters Q and B given by $Q = \bar{q}$ and $B = \bar{q^2} - \bar{q}^2 + \bar{b}$, respectively.

We now consider a superposition of the total line shapes $\sigma_j(\alpha)$ $(j = 1, \ldots, N)$ given by the product of the generalized Fano functions $\sigma_F^j(\alpha)$ and the corresponding background functions $\sigma_B^j(\alpha)$ as $\sigma_j(\alpha) = \sigma_B^j(\alpha)\sigma_F^j(\alpha)$. As discussed in Sec. II B, we are interested in the average of $\sigma_j(\alpha)$ written as

$$\bar{\sigma}(\alpha) = \frac{1}{N}\sum_{j=1}^{N} \sigma_j(\alpha) = \frac{1}{N}\sum_{j=1}^{N} \sigma_B^j(\alpha)\sigma_F^j(\alpha). \tag{11}$$

In the same way as before, we assume that the background functions can be expressed by a common function $g(\alpha)$ independent of j as $\sigma_B^j(\alpha) = u_j/g(\alpha)$, where u_j is the normalization factor given by $u_j = \sigma_B^j(\alpha_F)$ at the resonance position $\alpha = \alpha_F$. Combining this expression with that of $\sigma_F^j(\alpha)$, we can express as

$$\bar{\sigma}(\alpha) = \frac{1}{g(\alpha)}\sum_{j=1}^{N}\left(\frac{u_j}{N}\right)\left[\frac{(X+q_j)^2 + b_j}{X^2+1}\right]. \tag{12}$$

Setting $w_j = u_j/N$ and repeating the procedure used to derive Eq. (10) from Eq. (9), we finally obtain

$$\bar{\sigma}(\alpha) = \frac{W}{g(\alpha)}\frac{(X+Q)^2 + B}{X^2+1}. \tag{13}$$

It is now clear that the average (or superposition) of different Fano line shapes also becomes a Fano line shape characterized by the new parameters W, Q and B, under the conditions that α_F and Γ_F are common for all individual asymmetric line shapes and $\sigma_B^j(\alpha)$ can be described by the common function $g(\alpha)$.

The above conclusion is rigorous in the mathematical sense. However, in practice, the same conclusion is drawn from the fitting results of the $FEF(z_j, \alpha)$ spectra inside the WG1 layer as presented in Sec. II B, even though the spectra satisfy approximately the mathematical conditions. In fact, a close examination of Table III reveals that the values of α_F for the three sampling points are practically the same, while the value of Γ_F fluctuates to some extent; the fluctuation in Γ_F is less than $\pm 1.1\%$ relative to their average value. The inset of Fig. 6(a) shows that the normalized background functions $\sigma_B^{jN}(\alpha)$ differ from each other depending on the sampling position, but the differences are small in the vicinity of the Fano resonance. Although not shown here, the fitting results of the $FEF(z_j, \alpha)$ spectra of other sampling points inside the WG1 layer used to calculate the average spectrum show similar behaviors for the parameters α_F and Γ_F and the normalized background function. It is now clear that the average FEF spectrum can be fitted with the line shape function with sufficiently small errors, because the mathematical conditions imposed for $\sigma_F^j(\alpha)$ and $\sigma_B^j(\alpha)$ are fulfilled approximately.

According to the above mathematical results, Q and B parameters of the average line shape are given by $Q = \bar{q}$ and $B = \bar{q^2} - \bar{q}^2 + \bar{b}$, respectively, which can be calculated from the weights $w_j = \sigma_B^j(\alpha_F)/N$. Using the numerical results for $\sigma_B^j(\alpha_F)$, q_j and b_j, presented in Figs. 6(c), 6(d), and 6(e), respectively, and the total number of the sampling points $N = 600$, we calculated the averages $\bar{q}$, $\bar{q^2}$, and $\bar{b}$. The values of Q and B parameters obtained from the averages are 0.774 807 and 0.402 851, respectively. Comparing these values of Q and B with those of q and b obtained from the Fano fitting of the average spectrum (Table III), we find that the Q value agrees with the q value with a very small error of

less than 0.16% (of the q value) and that the B value deviates slightly from the b value with an error smaller than 2.72% (of the b value). These results indicate again that the mathematical relations hold approximately for the present FEF spectra. From the discussion given above, we can suggest that in practice, the Fano line shape generated by the superposition has a tolerance for the fluctuation in the resonance parameters and background functions of constituent Fano line shapes. Although such tolerance has not been discussed in detail in the literature, Fano line shapes in a variety of nanostructures may have been formed successfully under the situations similar to the present study.

D. Discussion

The present EM analyses reveal that the spectra of local electric fields at different positions inside the WG1 layer exhibit different Fano line shapes characterized by different values of the parameters q_j and b_j. From the point of view of propagation of EM waves, the distribution of local electric fields is established as a consequence of multiple reflection and transmission processes of the EM waves traveling back and forth inside the multilayer structure. Although the EM calculations allow us to know the field distributions for given structural parameters, from the EM results only, it is difficult to clarify the origins of the different Fano responses for different positions inside the waveguide layer. The coupled oscillator model has been used very frequently to describe the Fano resonances in nanostructures[6,20] and helped to clarify the mechanism of Fano line shape formation, i.e., the coupling between a broad (bright) EM mode and a sharp (dark) EM mode, which is formulated as the coupling of two harmonic oscillators. As demonstrated in our recent study,[21] the coupled oscillator model can describe fairly well the behavior of local electric fields inside the waveguide layers in the multilayer structure, in which two planar waveguide modes are coupled with each other. In our study, the averages of the local electric fields inside the two waveguide layers were correlated to the amplitudes of two oscillators and the behaviors of the average fields could be well reproduced by the solutions of coupled oscillator equations. However, the present results suggest the necessity of introducing many harmonic oscillators describing the local electric fields at different positions inside the WG1 layer instead of only one oscillator describing the average local field. According to the general classification of Fano resonances,[5,22] such a description is thought to correspond to the case of multiple Fano resonance generated by the interaction between multiple continua and a discrete state. Further studies are required to clarify the physical origin of the different Fano line shapes in the WG1 layer and the generation of a Fano line shape from a superposition of different Fano line shapes.

To examine whether the nested formation mechanisms of Fano line shape described above for the all-dielectric multilayer structure work in other Fano-resonant multilayer structures, we extended our EM calculations and line shape analyses to a metal-dielectric multilayer structure consisting of an Au layer, a SiO_2 spacer layer (S1 layer), and an Al_2O_3 waveguide layer (WG1 layer), integrated into an ATR geometry. The results are presented in the supplementary material. The structural parameters (thicknesses and refractive indices of the layers) assumed are quite different from those assumed in the above. In place of the PWG1 waveguide mode, a surface plasmon polariton (SPP) mode supported by the Au−SiO_2 interface (broad mode) is involved in the formation of the Fano line shape. Although the map of FEF (Fig. S2 in the supplementary material) and spectra of $FEF(\alpha)$ (Fig. S4 in the supplementary material) appear to be different from those of the all-dielectric multilayer structure due to the SPP mode involved, the results of analyses presented in the supplementary material (Figs. S3 and S5 in the supplementary material) clearly demonstrate the same nested formation mechanisms of the Fano line shape as summarized in Fig. 4. With the aid of the results presented in the supplementary material, we finally suggest that the nested formation mechanisms of Fano line shape are not limited to the all-dielectric multilayer structure considered but expected to work in a wide class of Fano-resonant multilayer structures.

III. CONCLUSION

The formation mechanism of the Fano line shape in the far-field ATR response of the coupled waveguide multilayer structure was studied in detail by tracing back to the behaviors of local electric fields generated inside the structure. Assuming a multilayer structure similar to those experimentally studied, electromagnetic calculations of reflectance R and distributions of local electric fields were performed. By fitting the far-field and local-field spectra to line shape functions, nested mechanisms of the Fano line shape formation hidden in the behaviors of local electric fields are revealed. First, the spectrum of absorption A that is directly connected to R by $A = 1 - R$ is shown to be composed of a Fano line shape and a Lorentzian line shape; the Fano line shape is generated by local absorption in one of the waveguide layers supporting a broad waveguide mode, while the Lorentzian line shape is generated by local absorption inside another waveguide supporting a sharp waveguide mode. Furthermore, it is shown that the Fano line shape arising from the local absorption inside the first waveguide layer is generated by a superposition of different Fano line shapes exhibited by local electric fields at different positions inside the waveguide layer. From mathematical considerations made on the line shape functions used to fit the spectra, we clarified the conditions under which the superposition of a Fano line shape and a Lorentzian line shape becomes a Fano line shape and the superposition of different Fano line shapes becomes a Fano line shape. Close examinations of the fitting parameters suggest that the spectral fitting is successful with small errors, even though the spectra analyzed satisfy only approximately the mathematical conditions. This result implies that in practice, the Fano line shape generated by the superposition of Fano and Lorentzian line shapes as well as that generated by the superposition of different Fano line shapes tolerate small fluctuations in the parameters of constituent line shapes. The formation mechanism of the Fano line shape revealed for the local absorption spectrum in the first waveguide layer suggests the necessity of introducing a physical model based on the multiple Fano resonance arising from the interaction between multiple continua with a discrete state. The results of additional EM calculations and spectral shape analyses performed for the metal-dielectric multilayer structure (found in the supplementary

material) support the same nested formation mechanisms of Fano line shape in the far-field ATR response.

SUPPLEMENTARY MATERIAL

See the supplementary material for results of EM calculations and line shape analyses performed for an $Au-SiO_2-Al_2O_3$ multilayer structure.

ACKNOWLEDGMENTS

This work was supported by the JSPS KAKENHI (Grant Nos. 19K05307 and 22K04967). M.F. acknowledges the support from Kobe University Strategic International Collaborative Research Grant (Type B Fostering Joint Research).

AUTHOR DECLARATIONS

Conflict of Interest

The authors have no conflicts to disclose.

Author Contributions

Shinji Hayashi: Conceptualization (lead); Data curation (lead); Funding acquisition (lead); Project administration (lead); Writing – original draft (lead); Writing – review & editing (lead). **Kengo Motokura:** Conceptualization (equal); Investigation (equal); Writing – review & editing (supporting). **Minoru Fujii:** Conceptualization (supporting); Project administration (lead); Writing – review & editing (equal). **Dmitry V. Nesterenko:** Conceptualization (supporting); Methodology (supporting); Writing – review & editing (supporting). **Zouheir Sekkat:** Conceptualization (supporting); Project administration (supporting); Writing – review & editing (equal).

DATA AVAILABILITY

The data that support the findings of this study are available from the corresponding author upon reasonable request.

REFERENCES

[1]B. Luk'yanchuk, N. I. Zheludev, S. A. Maier, N. J. Halas, P. Nordlander, H. Giessen, and C. T. Chong, "The Fano resonance in plasmonic nanostructures and metamaterials," Nat. Mater. **9**, 707 (2010).
[2]A. E. Miroshnichenko, S. Flach, and Y. S. Kivshar, "Fano resonances in nanoscale structures," Rev. Mod. Phys. **82**, 2257 (2010).
[3]M. F. Limonov, M. V. Rybin, A. N. Poddubny, and Y. S. Kivshar, "Fano resonances in photonics," Nat. Photonics **11**, 543 (2017).
[4]U. Fano, "Sulo spettro di assorbimento dei gas nobili presso il limite dello spettro d'arco," Nuovo Cimento **12**, 154 (1935).
[5]U. Fano, "Effects of configuration interaction on intensities and phase shifts," Phys. Rev. **124**, 1866 (1961).
[6]B. Gallinet and O. J. F. Martin, "Ab initio theory of Fano resonances in plasmonic nanostructures and metamaterials," Phys. Rev. B **83**, 235427 (2011).
[7]B. Gallinet and O. J. F. Martin, "Influence of electromagnetic interactions on the line shape of plasmonic Fano resonances," ACS Nano **5**, 8999 (2011).
[8]B. Gallinet and O. J. F. Martin, "Relation between near-field and far-field properties of plasmonic Fano resonances," Opt. Express **19**, 22167 (2011).
[9]I. Avrutsky, R. Gibson, J. Sears, G. Khitrova, H. M. Gibbs, and J. Hendrickson, "Linear systems approach to describing and classifying Fano resonances," Phys. Rev. B **87**, 125118 (2013).
[10]C. Ott, A. Kaldun, P. Raith, K. Meyer, L. Martin, J. Evers, C. H. Keitel, C. H. Greene, and T. Pfeifer, "Lorentz meets Fano in spectral line shapes: A universal phase and its laser control," Science **340**, 716 (2013).
[11]Q. Wang, Y. Huang, Z. Yao, and X. Xu, "Analysis of transition from Lorentz resonance to Fano resonance in plasmon and metamaterial systems," Opt. Quant. Electron. **48**, 82 (2016).
[12]Lj. Babić and M. J. A. de Dood, "Interpretation of Fano lineshape reversal in the reflectivity spectra of photonic crystal slabs," Opt. Express **18**, 26569 (2010).
[13]T. Fukuta, S. Garmon, K. Kanki, K. Noba, and S. Tanaka, "Fano absorption spectrum with the complex spectral analysis," Phys. Rev. A **96**, 052511 (2017).
[14]S. Mizuno, "Analytical expressions for real and complex Fano parameters in a simple classical harmonic oscillator system," Jpn. J. Appl. Phys. **61**, SG1010 (2021).
[15]B. Kang, K. Motokura, M. Fujii, D. V. Nesterenko, Z. Sekkat, and S. Hayashi, "Fano resonant behaviour of waveguide mode in all-dielectric multilayer structure directly monitored by fluorescence of embedded dye molecules," J. Opt. **21**, 105006 (2019).
[16]B. Kang, K. Motokura, M. Fujii, D. V. Nesterenko, Z. Sekkat, and S. Hayashi, "Observation of Fano line shape in directional fluorescence emission mediated by coupled planar waveguide modes and interpretation based on Lorentz reciprocity," AIP Adv. **10**, 075302 (2020).
[17]M. N. Polyanskiy, Refractive index database (2015), see http://refractiveindex.info/.
[18]C. C. Katsidis and D. I. Siapkas, "General transfer-matrix method of optical multilayer systems with coherent, partially coherent, and incoherent interface," Appl. Opt. **41**, 3978 (2002).
[19]L. D. Landau and E. M. Lifshitz, *Electrodynamics of Continuous Media*, 1st ed. (Pergamon Press, Oxford, 1960).
[20]B. Gallinet, *Fano resonances in Optics and Microwaves Physics and Applications*, Springer Series in Optical Sciences Vol. 219, edited by E. Kamenetskii, A. Sadreev, and A. Miroshnichenko (Springer, Cham, 2018), Chap. 5, p. 109.
[21]K. Motokura, M. Fujii, D. V. Nesterenko, Z. Sekkat, and S. Hayashi, "Coupling of planar waveguide modes in all-dielectric multilayer structures: Monitoring the dependence of local electric fields on the coupling strength," Phys. Rev. Appl. **16**, 064065 (2021).
[22]K. Ueda, "Spectral line shapes of autoionizing Rydberg series," Phys. Rev. A **35**, 2484 (1987).